
**AFRL-AFOSR-VA-TR-2022-0325**

# Exploration of Acoustically Coupled Combustion Instabilities Relevant to Rocket Propulsion Systems

**Karagozian, Ann**
**UNIVERSITY OF CALIFORNIA LOS ANGELES**
**11000 KINROSS AVE STE 102**
**LOS ANGELES, CA,**
**US**

**06/29/2022**
**Final Technical Report**



Air Force Research Laboratory
Air Force Office of Scientific Research
Arlington, Virginia 22203
Air Force Materiel Command

# REPORT DOCUMENTATION PAGE

**PLEASE DO NOT RETURN YOUR FORM TO THE ABOVE ORGANIZATION.**

| **1. REPORT DATE** | **2. REPORT TYPE** | **3. DATES COVERED** | |
|---|---|---|---|
| 20220629 | Final | **START DATE** 20190401 | **END DATE** 20220331 |

**4. TITLE AND SUBTITLE**
Exploration of Acoustically Coupled Combustion Instabilities Relevant to Rocket Propulsion Systems

| **5a. CONTRACT NUMBER** | **5b. GRANT NUMBER** | **5c. PROGRAM ELEMENT NUMBER** |
|---|---|---|
| | FA9550-19-1-0096 | 61102F |
| **5d. PROJECT NUMBER** | **5e. TASK NUMBER** | **5f. WORK UNIT NUMBER** |
| | | |

**6. AUTHOR(S)**
Ann Karagozian

**7. PERFORMING ORGANIZATION NAME(S) AND ADDRESS(ES)**
UNIVERSITY OF CALIFORNIA LOS ANGELES
11000 KINROSS AVE STE 102
LOS ANGELES, CA
US

**8. PERFORMING ORGANIZATION REPORT NUMBER**

| **9. SPONSORING/MONITORING AGENCY NAME(S) AND ADDRESS(ES)** | **10. SPONSOR/MONITOR'S ACRONYM(S)** | **11. SPONSOR/MONITOR'S REPORT NUMBER(S)** |
|---|---|---|
| Air Force Office of Scientific Research<br>875 N. Randolph St. Room 3112<br>Arlington, VA 22203 | AFRL/AFOSR RTA1 | AFRL-AFOSR-VA-TR-2022-0325 |

**12. DISTRIBUTION/AVAILABILITY STATEMENT**
A Distribution Unlimited: PB Public Release

**13. SUPPLEMENTARY NOTES**

**14. ABSTRACT**
Acoustically coupled combustion instabilities are among the most challenging and unpredictable problems in aerospace propulsion systems, and can result in large scale, potentially catastrophic pressure oscillations in liquid rocket engines (LREs).

**15. SUBJECT TERMS**

| **16. SECURITY CLASSIFICATION OF:** | | | **17. LIMITATION OF ABSTRACT** | **18. NUMBER OF PAGES** |
|---|---|---|---|---|
| **a. REPORT** | **b. ABSTRACT** | **c. THIS PAGE** | | |
| U | U | U | UU | 20 |

| **19a. NAME OF RESPONSIBLE PERSON** | **19b. PHONE NUMBER** *(Include area code)* |
|---|---|
| MITAT BIRKAN | 426-7234 |

**Final Report:**

**AFOSR Award No. FA9550-19-1-0096**

**Grant Period: 4/1/2019 – 3/31/2022**

**AFOSR Space Propulsion and Power Program**

Dr. Mitat Birkan, AFOSR/RTA, Program Manager

# Exploration of Acoustically Coupled Combustion Instabilities Relevant to Rocket Propulsion Systems

Prof. Ann R. Karagozian, Principal Investigator
Department of Mechanical and Aerospace Engineering
Energy and Propulsion Research Laboratory
University of California, Los Angeles

## Abstract/Overview

Acoustically coupled combustion instabilities are among the most challenging and unpredictable problems in aerospace propulsion systems, and can result in large scale, potentially catastrophic pressure oscillations in liquid rocket engines (LREs). A fundamental understanding of the interactions among flow and flame hydrodynamics, acoustics, and reaction kinetics is essential to determining combustor stability and controlling combustion processes. Under the support of this AFOSR grant, over the past three years our group at UCLA's Energy and Propulsion Research Laboratory (EPRL) has been pursuing fundamental experiments that can shed light on combustion instabilities and their control, including alternative injector configurations of relevance to Air Force LRE systems. Over the past three years we focused on gas-phase combustion created by several alternative injectors (single element, triple element, and coaxial geometries) in an acoustically resonant environment, primarily using gaseous methane (CH4) injected into air within a closed acoustic waveguide. Different diagnostics and analysis procedures for these acoustically coupled combustion studies included simultaneous phase-locked OH* chemiluminescence and high speed visible imaging, with the ability to quantify characteristic signatures associated with transitions in the flame dynamics. We additionally explored the use of Background-Oriented Schlieren (BOS) imaging to enable extraction of density gradients and propagation fronts in the reactive flowfield. Quantification of flame dynamics was achieved for time-resolved images via proper orthogonal decomposition (POD) and dynamic mode decomposition (DMD). Phase portraits associated with POD mode coefficient trajectories enabled development of characteristic signatures associated with different oscillatory flame states: sustained oscillatory combustion (SOC), periodic liftoff and reattachment (PLOR), and full-scale blowoff or blowout. The dynamics observed here were not only relevant to ongoing, larger scale experiments on round jet flames exposed to transverse excitation at AFRL/RQR, but the analysis tools developed by our group were implemented at AFRL by a UCLA student (and later postdoc) conducting similar experiments at AFRL. This very fruitful study enabled significant strengthening of collaborations with AFRL/RQR and defined a roadmap for future studies involving data driven dynamical characterization and reduced order modeling.

**Summary of Results: Dynamics of Gaseous Flame-Transverse Acoustic Coupling**

Ann R. Karagozian[a], Andres Vargas[b], Arin Hayrapetyan[b], H. S. Sim[c], Sarina Kiani[d], Miguel Plascencia[e] and Jose Guerrero[f]

Over the past several years our group has investigated the behavior of single as well as multiple (mostly triple) and coaxial gaseous fuel jets burning within a closed, optically-accessible cylindrical waveguide, operating at atmospheric pressure and with loudspeakers situated at each end of the waveguide (see **Figure 1(a)**). This configuration has been used in prior AFOSR-supported experiments involving liquid fuel droplets, including nanofuels (Sevilla, et al.[1],Bennewitz, et al.[2], Sim, et al.[3,4], Vargas, et al.[5]). In the gas-phase experiments, both methane and propane have been explored by our group, but a primary focus was on methane microjet flames and the response to external acoustic excitation in the form of standing waves, as this is a smaller scale version of ongoing experiments at AFRL/RQR at atmospheric and higher pressures (see Plascencia dissertation[6] and Plascencia, et al.[7,8]). Details on the experiment's operation, whereby the jet flames may be situated at various locations relative to the standing acoustic waves, in the vicinity of a pressure node (PN) or velocity antinode (VAN), are available in recent publications for the gaseous fuel jet experiments by our group (Sim, et al.[9] and Vargas, et al.[10]), and in the recent Ph.D. dissertation by Vargas[11]. The flexibly designed facility here involves the ability to move the speakers bounding the waveguide so that the flame can be studied at positions relative to the PN/VAN, and also enabling us to study alternative fuel injectors, including single, triple, and coaxial injectors, shown in **Figure 1(b).**

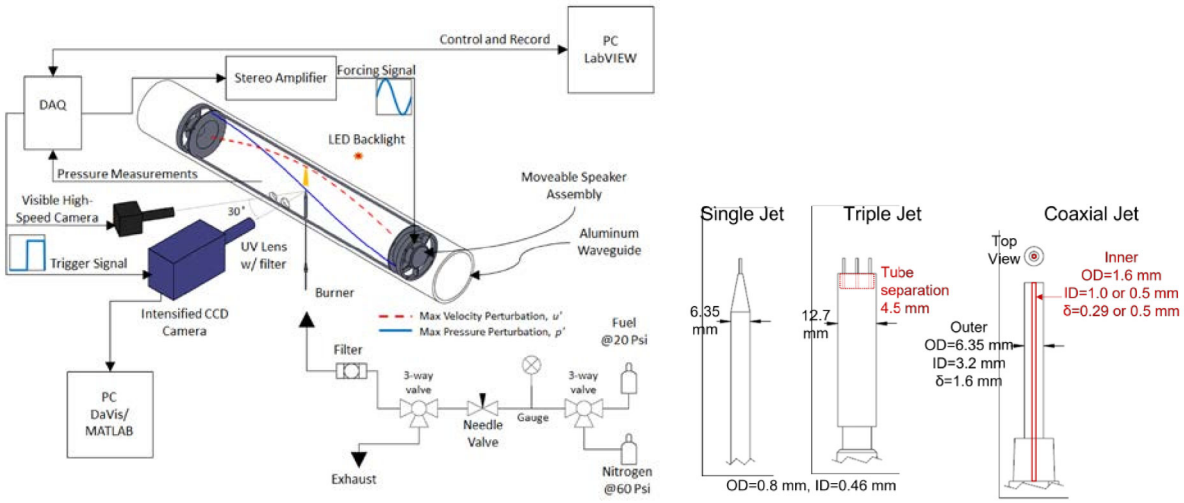


**(a)** **(b)**

**Figure 1. (a) Waveguide apparatus with movable speaker assembly and optical access for OH* chemiluminescence and high speed visible imaging of a gaseous laminar jet diffusion flames. (b) Alternative injectors explored in the experiments.**

[a] Professor, UCLA Department of Mechanical and Aerospace Engineering
[b] Ph.D. student, UCLA Department of Mechanical and Aerospace Engineering
[c] Postdoctoral Scholar, UCLA MAE Dept; currently Asst. Prof., Aerospace Engr., Sejong Univ., Seoul, South Korea
[d] M. S. student; currently engineer, Boeing Co.
[e] Ph.D student; currently NRC Postdoctoral Scholar, AFRL/RQR
[f] Undergraduate student, UCLA MAE Dept; currently, Ph.D. student, University of Michigan, Aerospace Engr.

**Single Flame-Acoustic Coupling Studies**

Single fuel jet experiments were carried out in the waveguide in the early part of this study, and have been documented in a journal paper[9]. These earlier studies focused on positioning the jet flame at locations away from the PN, so that bulk flame deflection was away from the geometric center, consistent with acoustic radiation force theory[1]. Simultaneous phase-locked, electronically excited hydroxyl radical (OH*) chemiluminescence and visible imaging, in addition to separate visible imaging at variable framing rates, were carried out using two cameras, a NanoStar intensified charge-coupled device (ICCD) camera and a high-speed monochrome camera, respectively. Details on these experiments are available in Sim, et al.[9] and in the Ph.D. dissertation of Andres Vargas[11], and are summarized here.

Phase-locked OH* chemiluminescence imaging of the oscillating single jet flame at a Reynolds number of 65 in the vicinity of a PN, with successively increasing excitation amplitudes, shows remarkable alterations in flame structure. **Figures 2 (a)-(d)** show a comparison of representative phase-locked OH* images, for excitation corresponding to maximum pressure perturbation amplitudes of 100, 150, 175, and 200 Pa, respectively. Here each image shown constituted an average of 250 OH* exposure shots, each phase-locked to 332 Hz and with each shot having an exposure time of 1/72 of the period (41.83 μs). At successively increasing amplitudes of excitation, from 100 to 175 Pa (Figs. 2(a)-(c)), more vigorous flame oscillations were observed, causing periodic shortening and elongation of the flame to a small degree, with clearer oscillations in the OH* intensity. At an even higher forcing amplitude, $p'_{max}$ = 200 Pa, phase-locked OH* images shown in Figure 2(d) suggested that the flames had transitioned into highly perturbed structures, with a non-coherent, seemingly 3D-like oscillatory geometry. During exposure to even higher forcing amplitudes, at or above $p'_{max}$ = 220 Pa, the flames were rapidly extinguished after a few seconds. Yet closer inspection of the shot-to-shot visible images at 200 Pa indicated that, for each phase-locked single image, there was considerable variation in the flame shape over the 250 images being averaged, in contrast to an essentially constant flame shape at a given phase for each of the images used in averaging at lower amplitude excitation conditions. For example, **Figure 2(e)** shows visible imaging of the phase evolution of the flame during same set of phase-locked experiments as in Figure 2(d), at 200 Pa forcing, but only showing the first shot (out of 250) used in the averaging. Significant variation in these visible images at a given phase in the course of the image acquisition at 200 Pa suggested there was additional oscillatory motion of the flame, not simply synchronized to 332 Hz. The phase-averaged images such as those in Figure 2(d) would only capture such motion as blurry flames. Yet data from phase-locked and shot-averaged images such as those in Figures 2(a)-(d) can be useful in quantifying many features of the acoustically-coupled combustion process, including measures of oscillations in flame position and lift-off, and calculation of the Rayleigh index associated with the oscillations in OH* chemiluminescence intensity and pressure. Rayleigh index, for example, shows a negative value for the high amplitude forcing case (Fig. 2(e)), corresponding to conditions where pressure and integrated chemiluminescence oscillations were out of phase. This metric could reveal information pertaining to the altered dynamics of the flame-acoustic coupling, and could be a useful signature as a preliminary measure of the transition in dynamics, albeit coarse. These and other parameters are described in Sim, et al.[9]

Additional high speed visible imaging (at approximately 1000 fps) was separately performed, without OH* imaging but at the same orientation angle as before, in order to quantify the methane microjet flames'

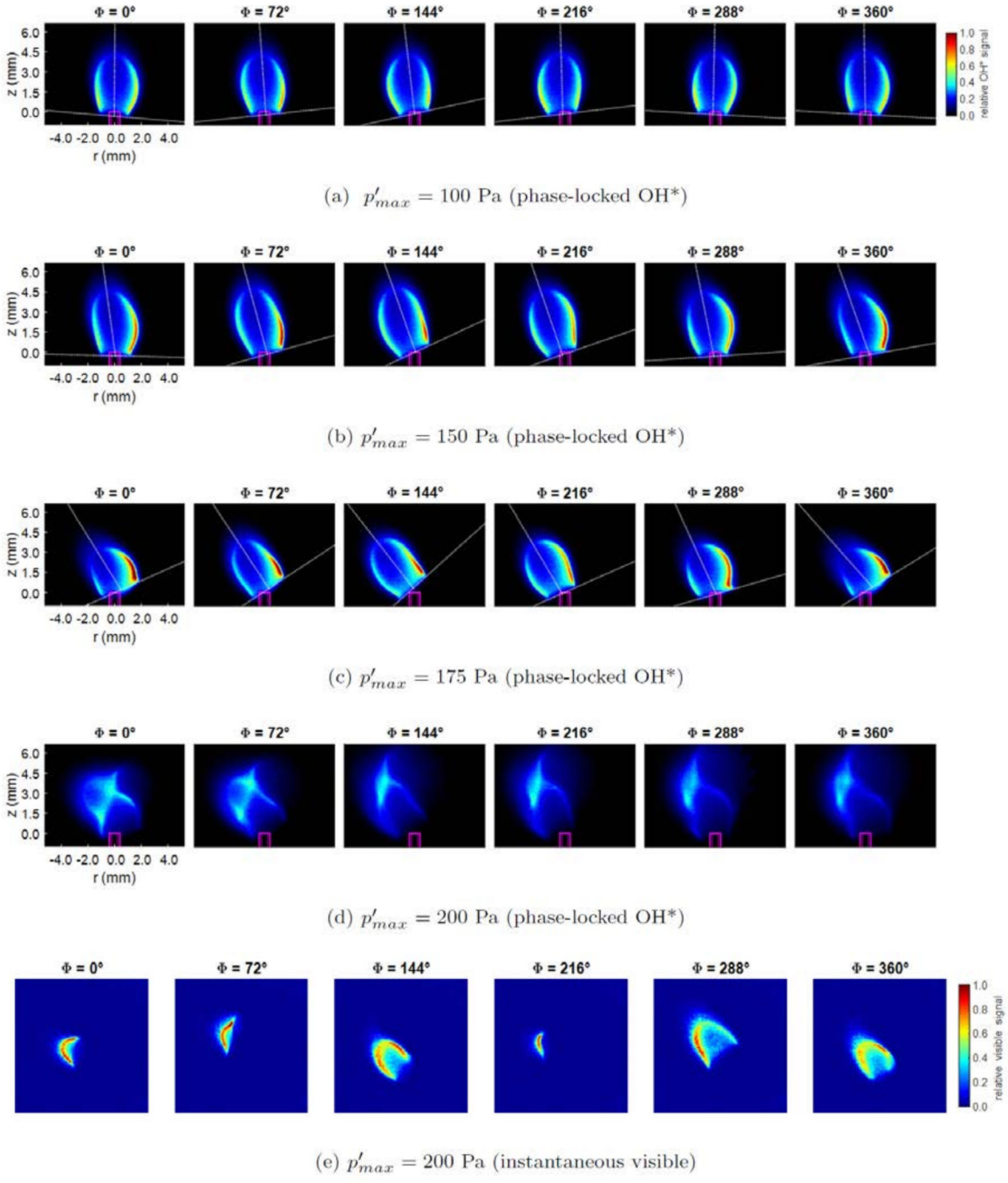


**Figure 2: Flame response to 332 Hz acoustic excitation as a function of phase of the acoustic cycle, for microjets located at x/λ = −0.029. (a)-(d) show phase-locked OH* chemiluminescence images (each averaged over 250 shots) for excitation amplitudes $p'_{max}$ = 100 − 200 Pa, respectively. (e) shows the first instantaneous shot of the visible images acquired at each phase, without averaging, for $p'_{max}$ = 200 Pa. From Sim, et al.[9]**

dynamical character more extensively via POD and DMD analysis. Such high speed visible imaging of the flames in the presence of acoustic excitation, enabling collection of multiple images in an actual acoustic cycle for 332 Hz excitation, enabled differences in flame dynamics dependent on forcing conditions to be observed and quantified. Such imaging demonstrated, as expected, that there was a relatively clean, repeatable periodic response of the microjet flame to excitation at a threshold amplitude of 175 Pa, where the dominant periodic flame structure appeared to correlate with the phase of the acoustic cycle. In contrast, the flame response to 332 Hz, 200 Pa forcing showed oscillatory behavior that involved additional, apparently much lower frequencies, in addition to smaller amplitude oscillations associated with the applied excitation frequency. Sample images taken over two cycles, for each of these forcing amplitudes, are shown in Figure 3. There was clear evidence that phase-locked imaging of the flame at 200 Pa would not be sufficient to resolve the important time scales in the flowfield, as there was no significant repeatability for the phases (relative to 332 Hz) indicated for that case.

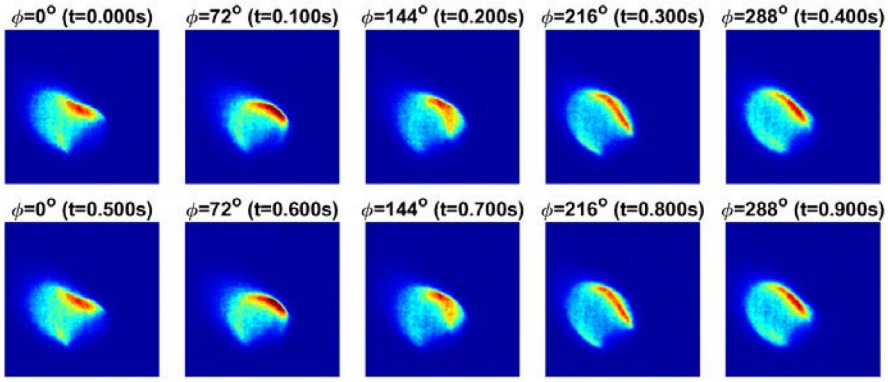


(a) $p'_{max}$ =175 Pa

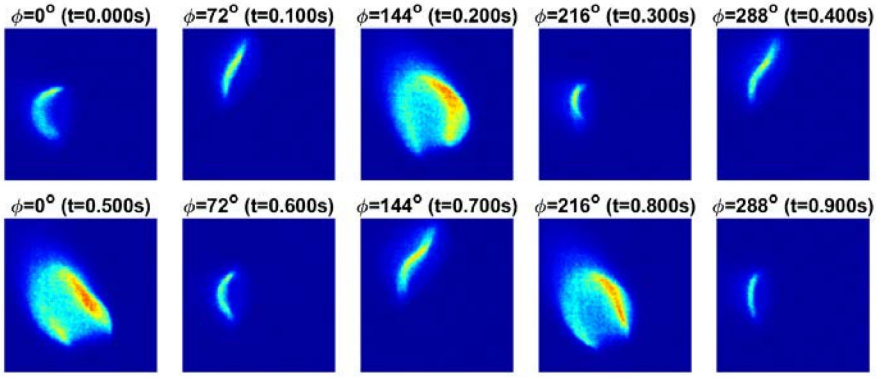


(b) $p'_{max}$ =200 Pa

**Figure 3: Time-series visible images of the flames over four sequential (non-phase-averaged) acoustic cycles, for 332 Hz excitation with amplitudes of (a) 175 Pa and (b) 200 Pa. Both phase $\phi$ and time $t$ from the initial image acquisition are shown for each instantaneous image. Data from Sim, et al.[9]**

Modal decomposition was applied to these time-series visible images via both proper orthogonal decomposition (POD) and dynamic mode decomposition (DMD). "Snapshot" POD may be used to extract mode structures from instantaneous snapshots of an oscillating flow, and thus was applied to the present time-series visible images of flame oscillations. POD enabled extraction of the most energetic modes

constituting the dynamics of flame-acoustic coupling, and thus proved useful in determining differences in dominant modes and dynamical character among differently excited jet flames. **Figure 4(a)**, for example, shows the first four POD mode structures and their corresponding percentage of the energy content for visible imaging of the single microjet exposed to a relatively low (100 Pa) excitation amplitude. These conditions correspond to the phase-locked OH* chemiluminescence images in Figure 2(a). Spectral analysis of the first POD mode produced a power spectral density (PSD) plot shown in **Figure 4(b)**, with a clear peak at the applied frequency, 332 Hz, suggesting a clear and direct locking-in of the oscillating flame to the applied acoustics. This lock-in was also demonstrated in some of the POD mode coefficient plots (e.g., the coefficients of POD mode 1 vs. those for mode 2, etc.) shown in **Figure 4(c)**. Beyond the mean jet flame's DMD structure (called DMD mode 1 here), the most prevalent frequency corresponded to mode 2, at 332 Hz, as shown in **Figure 4(d)**, with the next highest mode (3) corresponding to 336 Hz.

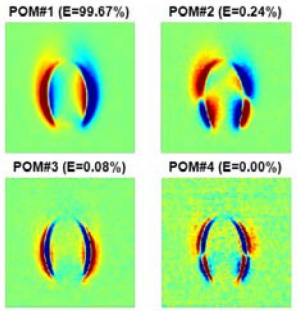


(a) POD Mode Structures

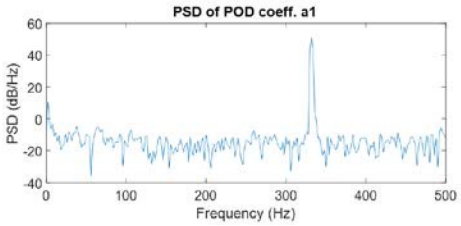


(b) PSD for POD mode 1

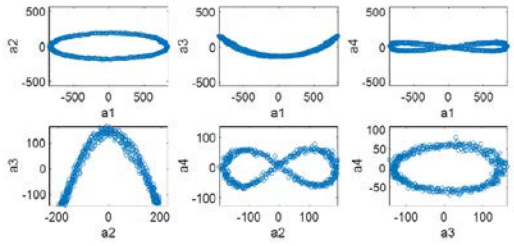

(c) POD mode coefficient plots

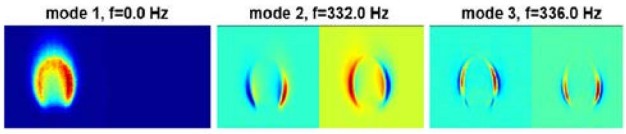


(d) DMD Mode Structures

**Figure 4: POD and DMD analysis results for 332 Hz excitation at an amplitude of 100 Pa for the single microjet at the location $x/\lambda = -0.029$. Results include (a) the first four POD mode structures with associated percentage of energetic content, and where the color denotes strength of the mode scaled by its own norm, (b) the power spectral density associated with the first POD mode, and (c) sample plots of the POD mode coefficients against one another for the first four modes. (d) shows mode structures for the first 3 DMD modes, where the left image corresponds to the real part and the right image corresponds to the imaginary part of the mode. Mode 1 corresponds to the mean flame structure. Data from Sim, et al.[9]**

With an increase in applied excitation amplitude for conditions where the flame oscillations in phase-locked OH* imaging appeared to be quite vigorous yet still regular and periodic (e.g., 175 Pa in Figure 2(c)), POD analysis produced modes that corresponded to flames that were more deflected in the mean, yet still cleanly oscillatory. This is shown in **Figure 5**. But the mode coefficient plots in Figure 5(c) showed distortion of the fairly symmetric phase plot shapes as compared with 100 Pa in Figure 4(c), suggesting a still-periodic behavior but one that may not be as simple as in the more symmetric oscillations at lower amplitude forcing. The asymmetries developing in the POD coefficient phase plots shown in Figure 5(c) are quite interesting, reminiscent of strange attractor-like shapes that can arise, for example, in phase space for reactive or non-reactive flows subjected to periodic acoustic forcing.

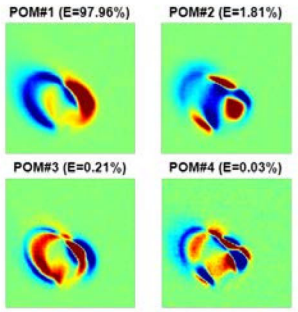


(a) POD Mode Structures

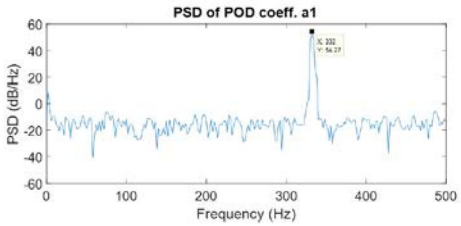


(b) PSD for POD mode 1

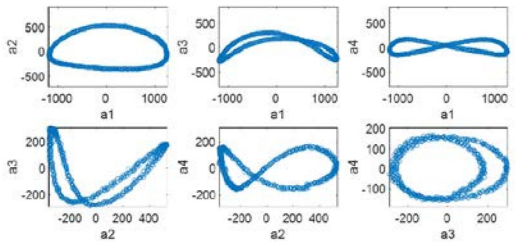

(c) POD mode coefficient plots

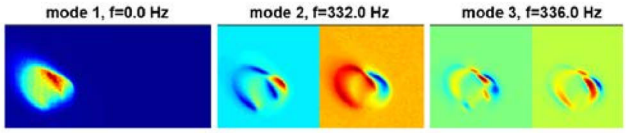


(d) DMD Mode Structures

**Figure 5: POD and DMD analysis results for 332 Hz excitation at an amplitude of 175 Pa for the single microjet at the location $x/\lambda = -0.029$. Results include (a) the first four POD mode structures with associated percentage of energetic content, and where the color denotes strength of the mode scaled by its own norm, (b) the power spectral density associated with the first POD mode, and (c) sample plots of the POD mode coefficients against one another for the first four modes. (d) shows mode structures for the first 3 DMD modes, where the left image corresponds to the real part and the right image corresponds to the imaginary part of the mode. Mode 1 corresponds to the mean flame structure. Data from Sim, et al.[9]**

Further increases in the forcing amplitude, to $p'_{max}$ = 200 Pa, demonstrated similar multiple frequencies associated with the oscillating flame, as shown in **Figure 6**. For this forcing condition, a low frequency mode at 14 Hz (with higher harmonics, shown for DMD modes 3 and 4) overtook the principal dynamics

of the oscillating flame, appearing to correspond to the strongly periodic lift-off of the flame, seen in both the high speed visible imaging and in the single shot phase-locked imaging for 200 Pa (Figure 2(e)). There was a transition in the POD coefficient plots in Figure 6(c), demonstrating altered phase trajectories reflective of the changing flame dynamics, again, worthy of exploration in the context of strange attractor geometries and an associated transition in combustion coupling. One could view these altered frequencies and mode shapes, and especially the altered phase plots, as characteristic signatures for this transition in flame dynamics. These and other results described in Sim, et al.[9] provide details on a range of such signatures for the single fuel jet, and ongoing studies for different single jet fuels, Reynolds numbers, and tube thicknesses are underway.

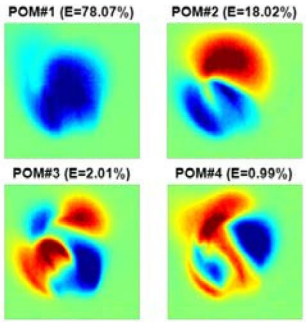


(a) POD Mode Structures

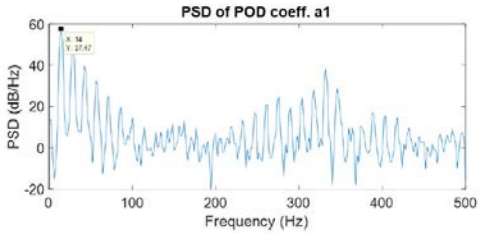


(b) PSD for POD mode 1

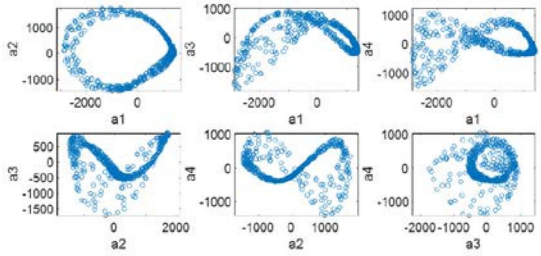


(c) POD mode coefficient plots

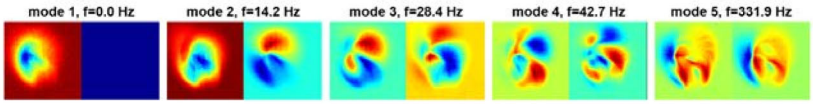


(d) DMD Mode Structures

**Figure 6: POD and DMD analysis results for 332 Hz excitation at an amplitude of 200 Pa for the single microjet at the location $x/\lambda = -0.029$. Results include (a) the first four POD mode structures with associated percentage of energetic content, and where the color denotes strength of the mode scaled by its own norm, (b) the power spectral density associated with the first POD mode, and (c) sample plots of the POD mode coefficients against one another for the first four modes. (d) shows mode structures for the first 3 DMD modes, where the left image corresponds to the real part and the right image corresponds to the imaginary part of the mode. Mode 1 corresponds to the mean flame structure. Data from Sim, et al.[9]**

More recently, additional high speed visible imaging (at approximately 1000 fps and 2000 fps) was separately performed, without OH* imaging, in order to quantify the methane microjet flames' dynamical characteristics and signatures associated with transitions at increasing excitation amplitudes; these transitions take the flames from sustained oscillatory combustion (SOC) at the excitation frequency to periodic liftoff and reattachment (PLOR) with the presence of much lower liftoff and reattachment frequencies to full scale flame blowoff. In earlier single jet dynamics with flames near the PN and with imaging at 1000 fps, POD and DMD analysis revealed that the most energetic modes during SOC took place at the applied frequency (in this case, 332 Hz), but with the next-highest mode at 336 Hz. The latter's unphysical observation resulted from the framing rate of the imaging; although the 332 Hz excitation is below the Nyquist frequency for such imaging, the potential for higher harmonics created aliasing that resulted in small 4 Hz and 336 Hz peaks in the power spectral density (PSD) results. At imaging with 2000 fps, the erroneous 336 Hz peak is eliminated from the spectral content for the lower modes. This study enables us to determine physical modes in the dynamics as compared with artifacts of the imaging; further results using both 1000 and 2000 fps have been acquired.

It is noted that the dynamics of the single laminar micro fuel jet are quite similar to those observed in the experiments by another UCLA Ph.D. student, Miguel Plascencia, in his recently completed studies[6] at AFRL/RQR, despite the fact that the Reynolds number range for the AFRL experiments is more than two orders of magnitude larger than that in the UCLA experiments. For example, **Figure 7** shows AFRL/RQR Schlieren imaging of the single jet at Reynolds number 5300 exposed to low-level acoustic excitation (local velocity perturbation around 8% of the jet velocity), resulting in SOC, with the highest 4 corresponding POD modes and representative POD mode coefficient plots. Many of the mode plots/phase portraits here are remarkably similar to those for the single jet at Re = 65, e.g., as shown in Figure 4, which has a velocity perturbation around 17% of the jet velocity. Hence analysis tools developed at UCLA have benefitted the AFRL studies.

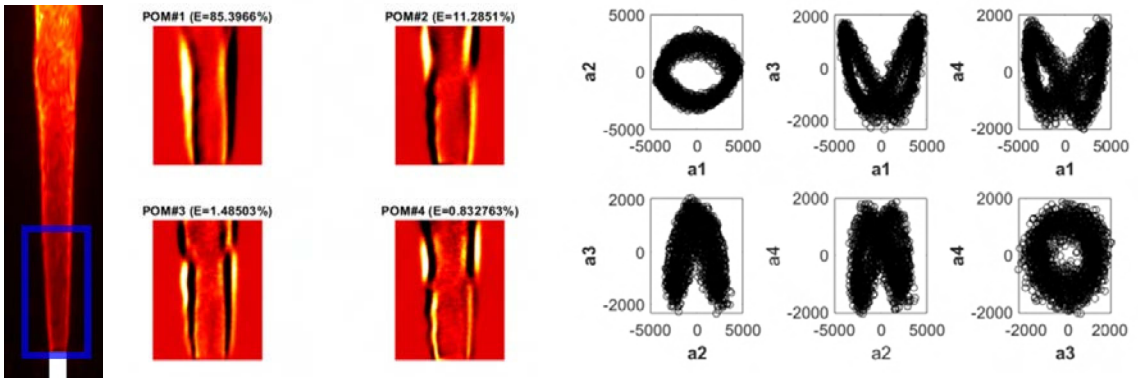


**(a)** **(b)** **(c)**

**Figure 7: For the single fuel jet exposed to low-amplitude acoustic excitation at frequency 581 Hz at a PN with local velocity perturbation 8% of the mean jet velocity, with jet Re = 5300. Shown are (a) Schlieren image of jet, (b) the first four POD mode structures with associated percentage of energetic content, and (c) sample plots of the POD mode coefficients against one another for the first four modes. Data from Plascencia[6].**

Additional imaging of single and multiple fuel jets has included incorporation of BOS to enable time-resolved visualization of the density field about the flame as well as extraction of velocity vectors based

on image-to-image front propagation. This imaging could take place at a much higher framing rate than for visible imaging, e.g., at 10,000 fps. Spectra extracted from the oscillatory velocity field are in progress. A sample BOS-based velocity field image is shown in **Figure 8**.

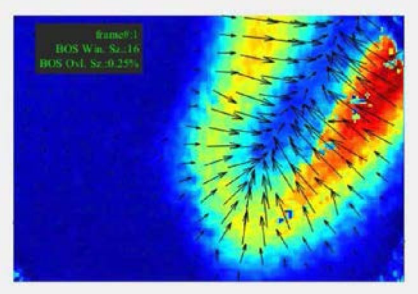

**Figure 8: Background-oriented Schlieren (BOS) imaging of the single fuel jet during periodic liftoff, with excitation fa at 332 Hz and p'max = 125 Pa, and with framing rate at 10,000 fps. Velocity vectors extracted from the density field are shown.**

Additional efforts for single and multiple jets involve development of reduced order models (ROMs) for the dynamical characteristics found in the POD modes; these efforts are being conducted in collaboration with Professor Leonardo Alves of the Universidade Federal Fluminense in Brazil[12]. It is important to note that, for SOC coupled behavior, relatively few POD modes are required to capture the essential dynamics of the flame-acoustic coupling, while many more modes are required to be included in the ROM when the dynamics include additional timescales, e.g., during PLOR when there are at least two dominant frequencies. This can be seen in the plot below, **Figure 9**, containing the cumulative POD mode energy contained in the single fuel jet dynamics for unforced, SOC, and PLOR behavior. While only 4 modes capture around 95% of the modal energetic content for SOC dynamics, over 13 modes are required to capture just 90% of the energy for PLOR.

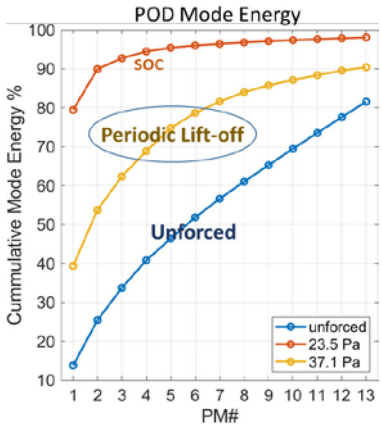


**Figure 9: POD modes energy distribution for the SOC and PLOR cases with forcing conditions at fa = 332 Hz and flame relative location x/λ = −0.029. The SOC case at local pressure perturbation amplitude 23.5 Pa shows that as few as 2 modes represent 90% of the cumulative mode energy, while for PLOR at 37.1 Pa as many as 13 modes are required. For the unforced flame, for which POD did not recover clear dynamics, many modes are required to represent the recorded data. From Vargas[11].**

**Triple Flame-Acoustic Coupling Studies**

Another focus of our experiments has been on the effect of acoustic perturbations on multiple fuel jets, such as the triple jet shown in Figure 1(b). This experimental study was documented in a conference paper[10] presented at the 12th U.S. National Combustion Meeting in May, 2021. The experiments utilized time-resolved high-speed visible imaging of the oscillatory flames to explore such dynamics and to quantify relevant metrics. Once again, POD was used to extract structural modes and phase diagrams associated with their temporal evolution. Three regimes were encountered based on the forcing amplitude: (1) at moderate forcing amplitudes, symmetric flame oscillations with linear coupling, (2) intermediate forcing with partial and periodic bulk flame lift-off (with some of the flame maintaining attachment and the opposite side of the injector periodically lifting off) and (3) highly perturbed periodic liftoff and flame reattachment with non-linear characteristics. For each regime, POD analysis revealed distinct signatures in their phase trajectories and power spectral density characteristics.

In contrast to recent findings at AFRL for triple flames, the present triple flames did interact with one another during acoustic excitation, especially at high amplitudes of excitation. Increasing the forcing amplitude acting on the triple flame led to asymmetric bulk deflection and periodic lift-off, as illustrated by the time-series snapshots in **Figure 10** for $p'_{max}$ = 175 Pa and 225 Pa. The bulk acoustic radiative force, which acts away from the PN, was observed to affect each of the three microjets to different degrees depending on the forcing amplitude. Lift-off of the flame occurred for only one injector for the lower amplitude forcing, but for nearly all three injectors at 225 Pa excitation. Time scales for these phenomena also differed among the different cases.

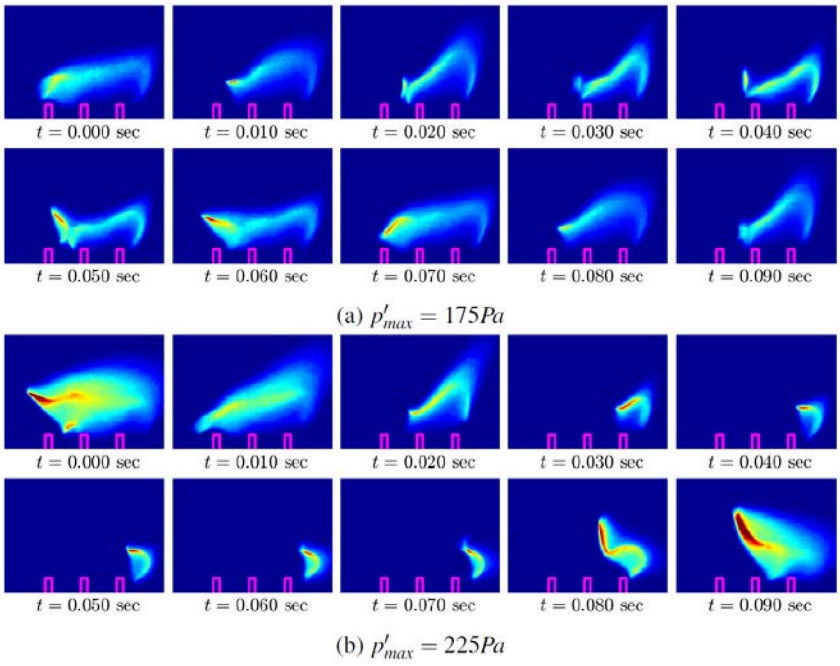


**Figure 10 Representative time-series images of triple microjet diffusion flames under acoustic forcing with x = 3 cm (jet to the right of the PN), fa = 332 Hz and different forcing amplitudes, (a) 175 Pa and (b) 225 Pa. Images from Vargas, et al.[10,11].**

With increasing forcing amplitudes, the transitions in the time-series images were accompanied by altered signatures in the POD analysis, as summarized by **Figures 11 and 12** for excitation at 175 Pa and 225 Pa, respectively. For the case of forcing with $p'_{max}$ = 175 Pa, Figure 11 shows that the cumulative total energy was somewhat more evenly distributed among the first four modes. The dominant frequency of this coupling was identified as 14 Hz, although quasi-periodicity with the forcing frequency (332 Hz), that is, with peaks at frequencies corresponding to linear combinations of 332 Hz and 14 Hz, was apparent in the PSD plots. In the case of forcing at an amplitude of 225 Pa, Figure 12 shows asymmetries developing in the POD phase trajectories, again reminiscent of "strange attractor"-like shapes. These and other test conditions are described in the Vargas dissertation[11].

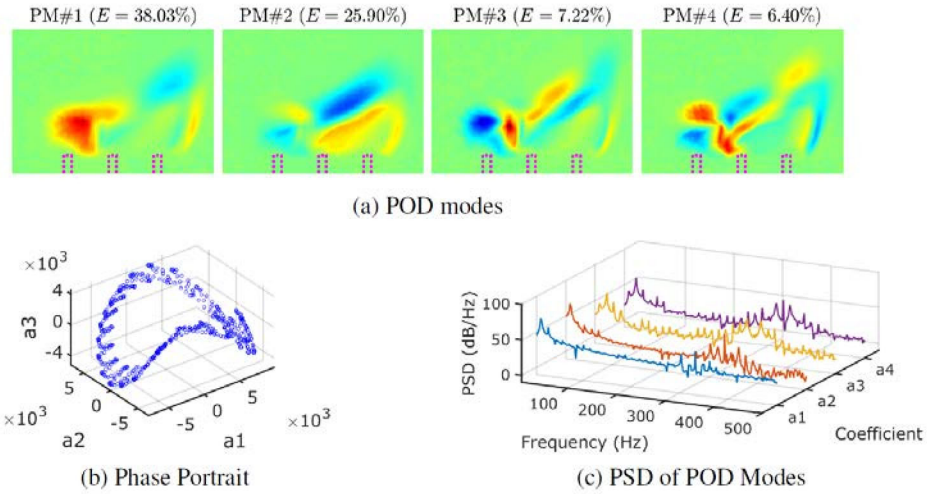


**Figure 11. POD analysis result for triple microjet diffusion flames under acoustic forcing with x = 3 cm, fa = 332 Hz and $p'_{max}$ = 175 Pa. Data from Vargas, et al.[10,11]**

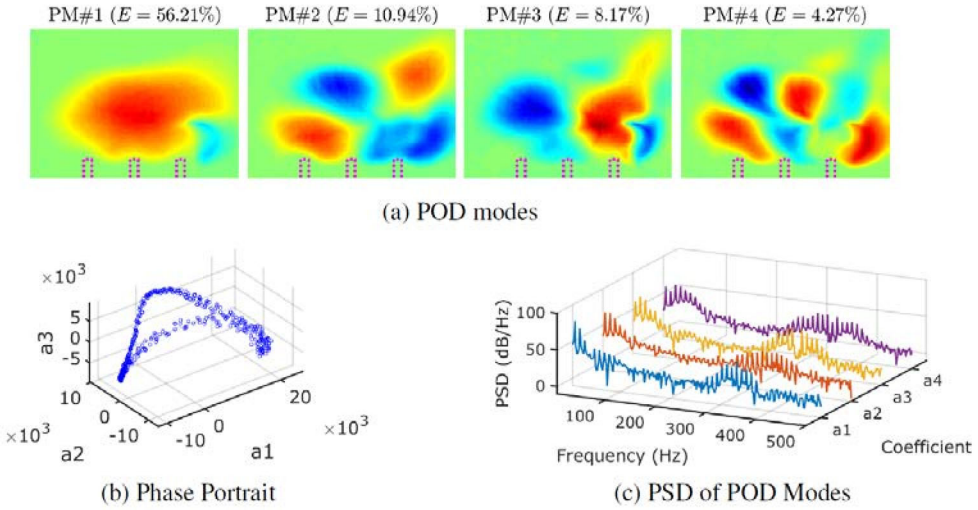


**Figure 12. POD analysis result for triple microjet diffusion flames under acoustic forcing with x = 3 cm, fa = 332 Hz and $p'_{max}$ = 225 Pa. Data from Vargas, et al.[10,11]**

More recently, a hybrid multi-scale POD (mPOD) method has been applied to extract spectrally cleaner modes. In mPOD, a filter bank is applied to the correlation matrix to split the data into non-overlapping portions in the frequency domain, each contribution is diagonalized to extract nearly orthogonal modes which are subsequently sorted and merged before finally enforcing orthogonality via QR factorization. The incorporation of mPOD enabled improvements in our understanding of the dynamical characteristics and signatures associated with transitions in these triple flame structures. For example, **Figure 13** shows various signatures in the POD analysis for the triple jet exposed to high enough excitation amplitude that periodic liftoff and reattachment takes place. Mode #1 resembled dynamics associated with the bulk lift-off of the leftmost flame, while mode #2 appeared to be a coupled mode with a distinct phase-difference (based on the elliptical phase portrait). The dominant frequency of this coupling was identified as f = 17 Hz, although quasi-periodicity with the forcing frequency (fa = 332 Hz), that is, with peaks at frequencies corresponding to linear combinations of 332 Hz and 17 Hz, was apparent in the PSD plots.

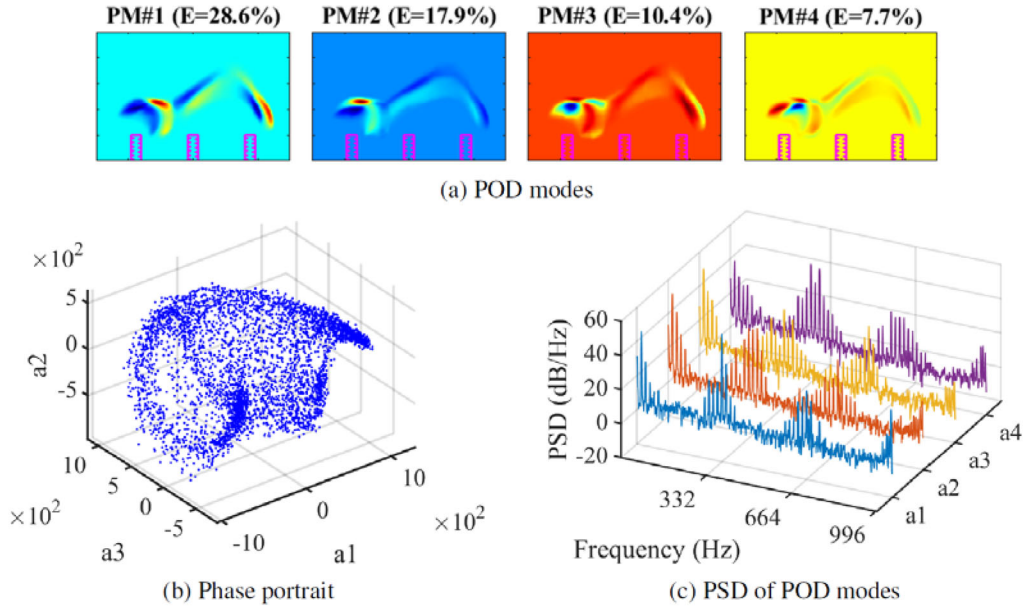


**Figure 13. POD analysis results for triple microjet diffusion flames under acoustic forcing with x = 3 cm, fa = 332 Hz and p'max = 150 Pa. Shown are (a) POD mode shapes for modes 1-4, (b) a sample phase portrait with POD mode coefficients a1, a2, and a3, and (c) PSD plots for the first 4 POD modes. Data from Vargas, et al.[10,11]**

Results for the multi-scale POD for the same conditions as in Figure 13, with excitation at 150 Pa, are shown in **Figure 14**. The 'pure' modes #2 and #3, with primary frequency f, exhibit localized flame dynamics in the vicinity of the left burner, consistent with the region of periodic lift-off. The mPOD mode #4 accentuates the presence of beat frequency phenomena due to a symmetric modulation of the 332 Hz frequency by the lift-off frequency. Additionally, mPOD phase trajectories appear more symmetric without the smearing effects observed in the regular POD phase portraits. Nevertheless, although the 'pure' mPOD modes structures are similar to the POD modes, their much lower relative energies suggests that the dynamics of the small-scale flame are best represented using fewer multi-frequency POD modes.

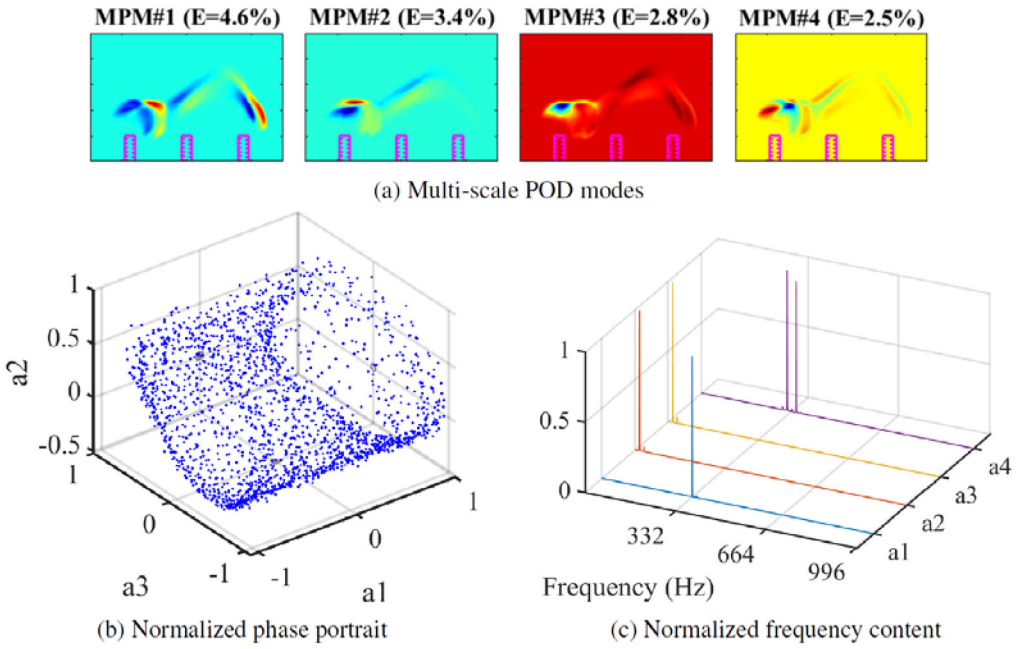


**Figure 14. Multi-resolution POD result for the same case as Figure 4 with p'max = 150 Pa. The coefficient and spectra values are normalized for qualitative comparison against regular POD. Data from Vargas, et al.[10,11]**

For cases that exhibit SOC flame response, the POD analysis suggests that a few modes can represent the dynamical system that models the flame response. It may be possible to derive the governing equation of a low-order model using the approach outlined by Kutz et al.[13] also known as Sparse Identification of Nonlinear Systems (SINDy). Following their formulation, Vargas[11] pursued its application to the problem of representing the triple jet dynamics with just a few (4) modes. Systematically adjusting the threshold α and the sine-fitting parameters created a solution, although in the present results it was valid only a few cycles before the model diverged as shown in **Fig. 15.** Separate ROM development by our collaborator at the UFF in Brazil, Prof. Leo Alves, utilizes a newly developed Topology Based Oscillatory Nonlinear Equations (TBONE) approach, which shows greater promise.

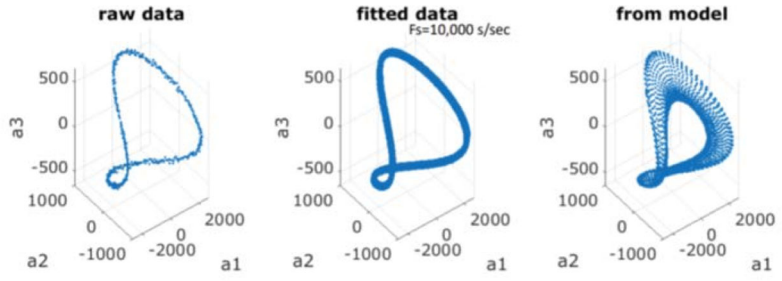


**Figure 15. Example of the application of the SINDy technique for modeling the data dynamical system represented by the first four POD modes for a burning triple jet imaged at 1000 FPS with acoustic forcing at p′ = 18.2 Pa, with fa = 332 Hz and located at xλ = −0.029. On the left is the raw data temporal modes obtained from POD, in the middle is the sine-model fit, and on the right is the solution from the identified model. Data from Vargas.[11]**

**Coaxial Jet Flame-Acoustic Coupling Studies**

A further focus of our recent experiments has involved coaxial jets, with air in the outer annular section and methane in the inner section, in addition to a few cases with the reverse situation. The behavior of such reactant injector-based flames in the presence of acoustic excitation is explored for flames in the vicinity of the PN. Several alternative geometries are examined for the coaxial jet, with different wall/tube thicknesses and annular-to-inner jet area ratios. The alternative geometries are shown in **Figure 16**, for the SAR-Thin, MAR-Thick and LAR-Thin injectors, the naming convention describing the area ratio $A_2/A_1$ and the inner tube wall thicknesses; these are similar to naming conventions used in coaxial jet studies performed at the Air Force Research Laboratory. The coaxial burner configuration consists of two concentric tubes, where the outer tube was kept the same among the three burners, and the inner tube's thickness and inner diameters were varied as shown.

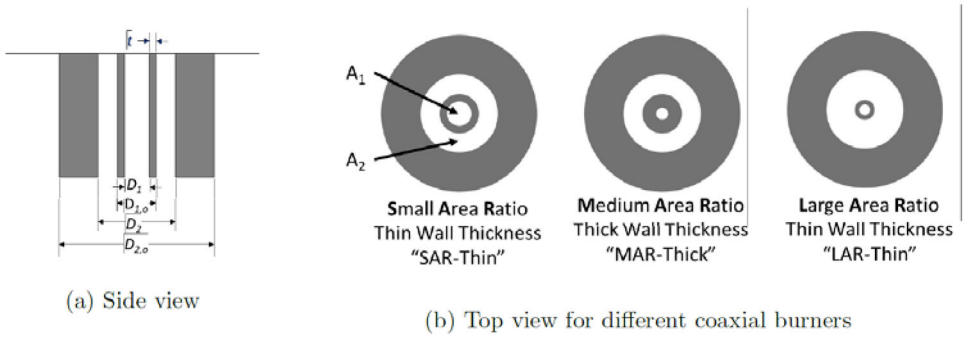


**Figure 16. The coaxial burner configuration from the side (a) and from the top, showing SAR-Thin, MAR-Thick and LAR-Thin injector geometries.**

Extensive datasets were taken (primarily high speed visible imaging) and POD analysis was applied for the three different injectors at different values of inner jet Reynolds number, annular-to-inner jet velocity ratio R, and volume flow rates, and are documented in the dissertation of Vargas[11]. While many of the trends for flame-acoustic coupling in the coaxial jets were similar to those for the other burners, tube thickness and velocity ratio R had rather significant effects on flameholding and transitioning from SOC to PLOR and then to full-scale blowoff. Phase portraits also evolved during increasing excitation amplitudes, as observed, for example, in the SAR-Thin injector shown in **Figure 17**. As in the prior single and triple jet experiments, there is a sudden change in the energy content of the first mode upon transition from SOC to PLOR; between Figs. 17b and 17c the energy of the first mode is reduced from 81% to 60%, while the energetic content of modes 2 and above increased, as with other burner configurations, associated with the additional timescale (or frequency) associated with periodic liftoff and reattachment. This observation implied that a greater number of modes was required to characterize the dynamics of flames undergoing PLOR as compared with SOC, for example.

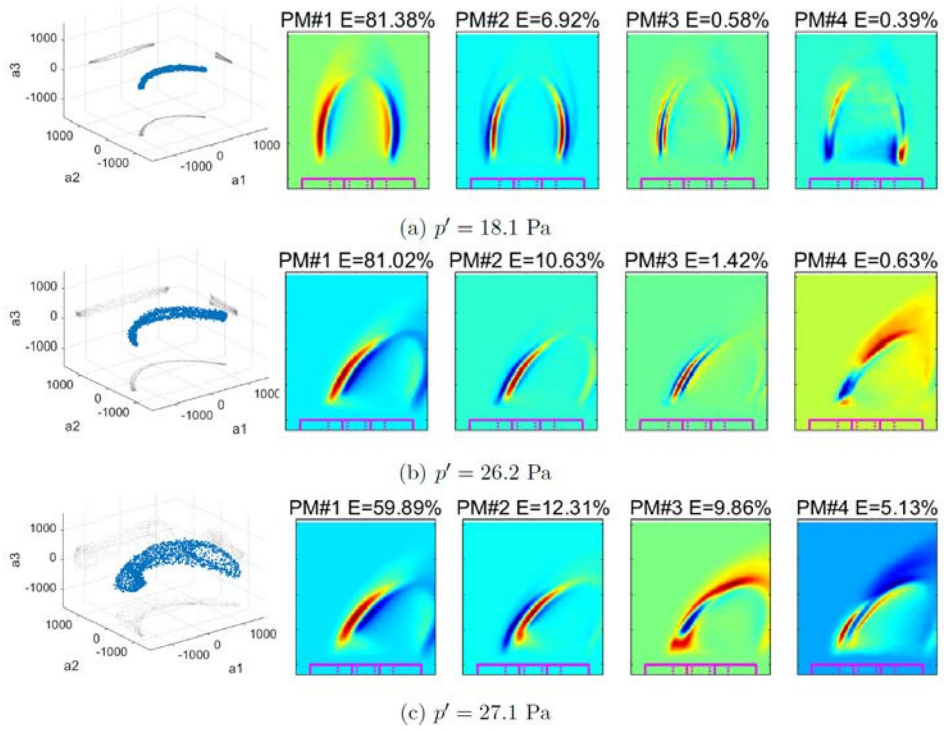


**Figure 17. POD modes and phase portraits for the acoustically perturbed flame associated with the SAR-Thin coaxial burner with Re = 40 and R = 0.3 and located at x/λ = −0.029 with respect to the PN location. The acoustic forcing frequency was fa = 332 Hz. Data from Vargas.[11]**

In addition to phase portraits as characteristic signatures for different coaxial jet flame dynamics, the alterations in the dominant frequency (transitioning from the applied frequency 332 Hz to the periodic liftoff frequency) can be used to distinguish injector characteristics. For example, as shown in **Figures 18ab**, Interestingly, at the higher annular-to-jet velocity ratio of R=2, with natural lift-off, there was no evidence of periodic flame reattachment. These findings suggest that with a higher R value the range of forcing amplitudes that lead to a PLOR transition is diminished.

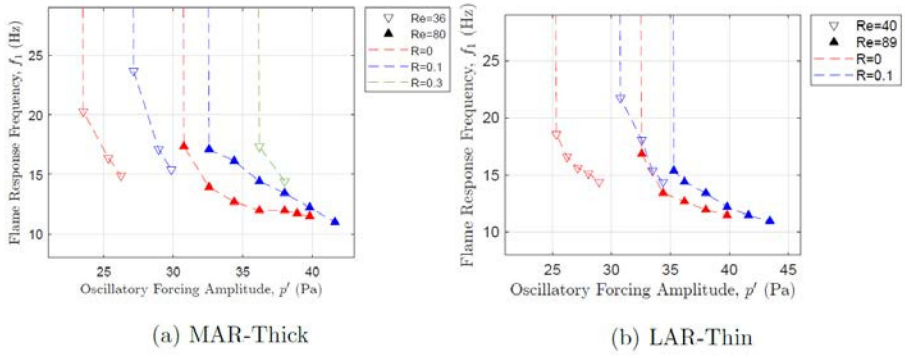


**Figure 18. Dominant frequency, $f_1$, extracted from POD mode #1 of the PLOR flame response under acoustic excitation with fa = 332 Hz for the MAR-Thick and LAR-Thin burners located at x/λ = −0.029 as a function of excitation amplitude, p′. The colored lines correspond to different R values. Data from Vargas[11].**

Finally, we note that the dynamical character for many of our acoustically coupled coaxial reactive jet experiments at very low Reynolds numbers were very similar to those associated with AFRL/RQR experiments for coaxial jets but at Reynolds numbers that were two orders of magnitude higher. **Figure 19** shows a comparison of UCLA-based and AFRL-based coaxial jet dynamics for SOC conditions, as but one example of this consistency in the characteristics. Additional comparisons between UCLA and AFRL/RQR experimental findings are described in the M.S. thesis of Sarina Kiani[14].

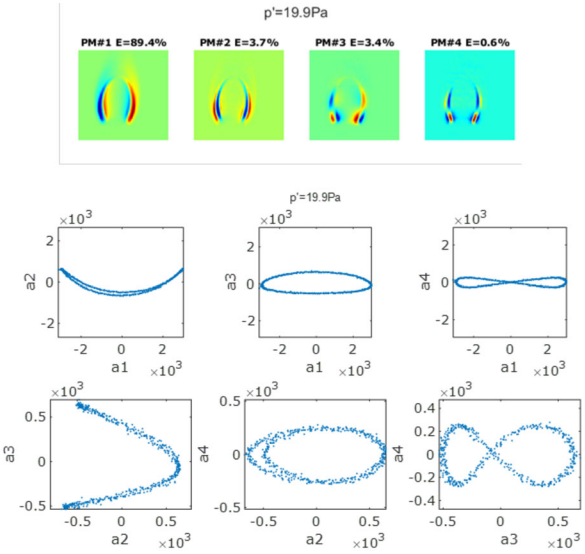


**(a) UCLA coaxial jet dynamics near a PN, Re ~ 80**

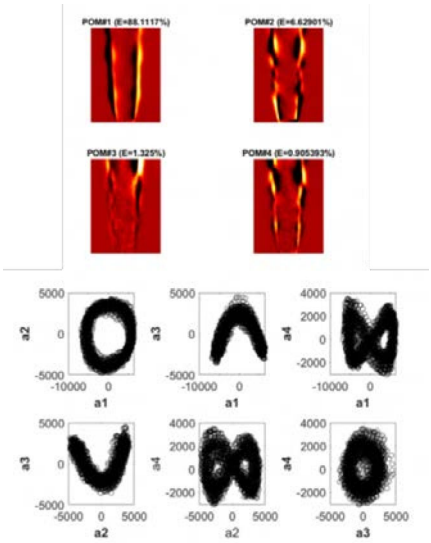


**(b) AFRL/RQR coaxial jet dynamics at the PN, Re = 5300**

**Figure 19. POD modes and phase portraits for the acoustically perturbed flame associated with (a) UCLA experiments for the SAR-Thin coaxial burner with Re ~ 80 and R = 0.3 and located at x/λ = −0.029 with respect to the PN location (data from Vargas[11]), and (b) AFRL/RQR experiments for the coaxial jet at a PN with Re = 5300 (data from Plascencia[6]).**

## Conclusions and Future Research Directions

Overall, these acoustically-coupled combustion experiments have revealed a great deal about the nature of nonlinear dynamics associated with combustion instabilities. The observed phenomena, as well as the analysis tools here, can have value for a range of future aerospace propulsion systems.

Given the intriguing differences in flame response among burner geometries and flow conditions, it is clear that there should be a future focus on additional experiments that explore jets with different geometries and wall thicknesses to determine the mechanisms that sustain the PLOR dynamics, to create a more direct correlation of the characteristic signatures associated with POD mode-based phase portraits and the dynamical state of the combustion process.

These experiments additionally would benefit from improvement in the denoising methods of imaging. Currently, the extraction of valid POD modes is subject to proper denoising of the flame images which was optimized through trial and error with a priority on the appearance and correspondence of the mode structures and energies, rather than focusing on their effect on temporal dynamics, and as such are more time-consuming than likely is necessary. Further insights may also be gained from evolving or deriving reduced-order models from the data, for example, using the Sparse Identification of Nonlinear Dynamics (SINDy) approach, as outlined for triple jet studies, or by making use of the topologies observed in the phase trajectories, as is being pursued by Prof. Leonardo Alves and his group at the Universidade Federal Fluminense.

**Bibliography: UCLA Publications and Presentations during this AFOSR grant period**

**Ph.D. dissertations and M.S. thesis**

- Plascencia Quiroz, M. A., "Combustion Dynamics of Liquid Droplets and Turbulent Jets Relevant to Rocket Engines", Ph.D. dissertation, UCLA, June 2021
- Kiani, Sarina, "Comparison of Acoustically Coupled Combustion Studies Under Laminar and Turbulent Conditions", M.S. Thesis, UCLA, November, 2021
- Vargas, Andres, "Acoustically Coupled, Non-Premixed Combustion Processes", Ph.D. dissertation, UCLA, July 2022

**Journal papers**

- Sim, H. S., Vargas, A., Ahn, D. C., and Karagozian, A. R., "Laminar Microjet Diffusion Flame Response to Transverse Acoustic Excitation", ***Combustion Science and Technology***, 2020 (invited). DOI: 10.1080/00102202.2020.1726897.
- Mok, Thalia, Harris, Elijah, Vargas, Andres, Afshar, Yalda, Han, Christina S., Karagozian, Ann, and Rao, Rashmi, "Evaluation of Respiratory Emissions During Labor and Delivery: Potential Implications for Transmission of Severe Acute Respiratory Syndrome Coronavirus 2 (SARS-CoV-2)", ***Obstetrics & Gynecology***, September 9, 2021 - Volume - Issue - 10.1097/AOG.0000000000004533 doi: 10.1097/AOG.0000000000004533 [**RESEARCH BASED ON REQUEST FROM UCLA HOSPITAL DURING COVID-19 PANDEMIC**]]

**Conference papers**

- Vargas, A., Guerrero, J., and Karagozian, A. R.*, "Laminar Flame Dynamics of Multi-Port Fuel Jets Under Acoustic Forcing", Paper 111001Q-000, accepted for presentation at the Western States Section/The Combustion Institute Spring 2020 meeting, Stanford California, March, 2020 [**POSTPONED DUE TO COVID-19 PANDEMIC**]
- Vargas, A., Kiani, S., and Karagozian, A. R., "Dynamics of Multi-Port Jet Diffusion Flames Under Acoustic Forcing", Paper 3E01, 12th U.S. National Combustion Meeting, May, 2021.

**Conference presentations (abstract only)**

- Karagozian, A. R., "Laminar Microjet Diffusion Flame Response to Transverse Acoustic Excitation", presented at the Symposium in Honor of Prof. William Sirignano, UC Irvine, September 6, 2019 (invited).
- Andres Vargas, Jose Guerrero, Ann Karagozian, and Hyung Sub Sim, "Acoustically-Coupled Combustion Dynamics of Laminar Microjet Diffusion Flames", presented at the American Physical Society/Division of Fluid Dynamics Meeting, Seattle, WA, November, 2019.
- Vargas, A., Guerrero, J., Kiani, S., and Karagozian, A. R., "Laminar Flame Dynamics of Multi-Port Fuel Jets Under Acoustic Forcing", presented at the American Physical Society/Division of Fluid Dynamics Meeting, remote conference, November, 2020
- Alves, L., Vargas, A., and Karagozian, A. R., "On the Development of Reduced Order Models for the Prediction of Acoustically Forced Laminar Diffusion Methane Flame Lift Off", presented at the American Physical Society/Division of Fluid Dynamics Meeting, remote conference, November, 2020

- Vargas, A., Kiani, S., and Karagozian, A. R., "Acoustically Excited Laminar Jet Diffusion Flames", presented at the 14th Southern California Flow Physics Symposium, April 10, 2021
- Vargas, A., Kiani, S., and Karagozian, A. R., "Laminar Flame Dynamics of Coaxial Methane-Air Jets Under Acoustic Forcing", presented at the American Physical Society/Division of Fluid Dynamics Meeting, Phoenix, AZ, November, 2021

## Report References


[1] Sevilla-Esparza, C. I., Wegener, J. L., Teshome, S., Rodriguez, J. I., Smith, O. I., and Karagozian, A. R., "Droplet Combustion in the Presence of Acoustic Excitation", ***Combustion and Flame***, Vol. 161, pp. 1604-1619, 2014.

[2] Bennewitz, J., Valentini, D., Plascencia, M., Vargas, A., Sim, H. S., Lopez, B., Smith, O. I., and Karagozian, A. R., "Periodic Partial Extinction in Acoustically Coupled Fuel Droplet Combustion", ***Combustion and Flame,*** Vol. 189, pp. 46-61, 2018.

[3] Sim, H. S., Plascencia, M. A., Vargas, A., Bennewitz, J. W., Smith, O. I., and Karagozian, A. R., "Effects of Inert and Energetic Nanoparticles on Burning Liquid Ethanol Droplets", ***Combustion Science and Technology,*** 2018. DOI: 10.1080/00102202.2018.1509857

[4] Sim, H. S., Plascencia, M. A., Vargas, A., and Karagozian, A. R., "Acoustically-Forced Droplet Combustion of Liquid Fuel with Reactive Aluminum Nanoparticulates", ***Combustion Science and Technology***, 2019. DOI: https://doi.org/10.1080/00102202.2019.1593971

[5] Vargas, A., Sim, H. S., Plascencia, M., and Karagozian, A. R., "Effect of aluminum nanoparticle additives on sooting hydrocarbon fuel droplet combustion", Paper 3G04, 11th U.S. National Combustion Meeting, Pasadena, California, March, 2019.

[6] Plascencia Quiroz, M. A., "Combustion Dynamics of Liquid Droplets and Turbulent Jets Relevant to Rocket Engines", Ph.D. dissertation, UCLA, June 2021.

[7] Plascencia, M. A., Roa, M., Karagozian, A. R., and Talley, D. G., "Turbulent Nonpremixed Jet Flames under Transverse Acoustic Forcing", Paper AIAA-10.2514/6.2020-3905, AIAA Propulsion & Energy Conference, August, 2020.

[8] Plascencia, M. A., Roa, M., Karagozian, A. R., Munipalli, R., and Talley, D. G., "Response of Gaseous Coaxial Turbulent Jet Combustion to Transverse Acoustic Forcing", presented at the AIAA Propulsion & Energy Conference, August, 2021.

[9] Sim, H. S., Vargas, A., Ahn, D. C., and Karagozian, A. R., "Laminar Microjet Diffusion Flame Response to Transverse Acoustic Excitation", ***Combustion Science and Technology***, 2020 (invited). DOI: 10.1080/00102202.2020.1726897.

[10] Vargas, A., Kiani, S., and Karagozian, A. R., "Dynamics of Multi-Port Jet Diffusion Flames Under Acoustic Forcing", Paper 3E01, 12th U.S. National Combustion Meeting, May, 2021.

[11] Vargas, Andres, "Acoustically Coupled, Non-Premixed Combustion Processes", Ph.D. dissertation, UCLA, July 2022

[12] Alves, L., Vargas, A., and Karagozian, A. R., "On the Development of Reduced Order Models for the Prediction of Acoustically Forced Laminar Diffusion Methane Flame Lift Off", presented at the American Physical Society/Division of Fluid Dynamics Meeting, remote conference, November, 2020

[13] Kutz, J. Nathan et al. (2016). Dynamic Mode Decomposition. Philadelphia, PA: ***Society for Industrial and Applied Mathematics***. isbn: 978-1-61197-449-2. doi: 10 . 1137 / 1 .9781611974508

[14] Kiani, Sarina, "Comparison of Acoustically Coupled Combustion Studies Under Laminar and Turbulent Conditions", M.S. Thesis, UCLA, 2021.